

Timing performance of SiPM-on-Tile elements: Laboratory and test beam measurements

F. Hummer^{a,b,1} L. Emberger^b F. Simon^{a,b}

^a*Institute for Data Processing and Electronics, Karlsruhe Institute of Technology,
Hermann-von-Helmholtz-Platz 1, 76344 Eggenstein-Leopoldshafen, Germany*

^b*Max-Planck-Institut für Physik,
Boltzmannstr. 8, 85748 Garching, Germany*

E-mail: fabian.hummer@kit.edu

ABSTRACT: The SiPM-on-Tile technology for highly granular calorimeters, where small plastic scintillator tiles are directly read out with SiPMs, has been developed for the CALICE Analog Hadron Calorimeter, and has been adopted for parts of the hadronic section of the CMS High Granularity Calorimeter. For future electron-positron colliders, a single cell time stamping on the sub-nanosecond level for energy deposits corresponding to single minimum-ionizing particles is desired to provide background rejection and to support pattern recognition and energy reconstruction with particle flow algorithms. To better understand the intrinsic time resolution achievable with the SiPM-on-Tile technology, we have performed detailed measurements in test beams at DESY, probing scintillator tiles of different sizes. The study is complemented by laser measurements that provide insights into processes within the scintillator tile relevant for timing. In this publication, we will discuss our measurement methods and the results of our SiPM-on-Tile timing study.

¹Corresponding author.

Contents

1	Introduction	1
1.1	Experimental Equipment	2
1.2	Breaking Down the Signal Creation	3
2	Test Beam Measurements	3
2.1	Experimental Setup	4
2.2	Results: Light Yield	4
2.3	Results: Time Resolution	6
3	Timing Properties of BC408	8
3.1	Experimental Setup	9
3.2	Results	10
4	Laser Measurements	11
4.1	Experimental Setup	12
4.2	Results: Light Detection and Hardware Response	13
4.3	Results: Light Collection	13
5	Conclusions	14

1 Introduction

Timing in event and shower reconstruction has become one of the main directions in calorimeter development and shows promising potential for the improvement of energy resolution in highly granular hadronic calorimeters [1–3]. High-precision time information allows to characterise the evolution of particle showers with the aim to identify shower components. Other uses of timing in calorimetry include background and pileup suppression, as well as the search for new long-lived particles.

A Silicon Photomultiplier (SiPM) is a 2D array of avalanche photodiodes operated in parallel and read out via one electric connection. Their very small size, the high photon detection efficiency and fast response make SiPMs very attractive for high-energy physics experiments, resulting in wide-spread use [4].

The SiPM-on-Tile technology has been developed for the CALICE Analog Hadron Calorimeter (AHCAL) [5], and has been adopted for parts of the hadronic section of the CMS High Granularity Calorimeter (HGCal) [6]. The plastics scintillator tiles are square-shaped, wrapped in reflective foil, and are directly placed on a PCB which hosts the SiPMs and the front-end electronics. A central dimple in each tile houses the SiPM which reads out the light from that tile directly. This

configuration is optimised for light collection and allows automatic assembly with a glue dispenser and a pick-and-place machine.

To better understand the intrinsic time resolution achievable with the SiPM-on-tile technology, we have performed detailed measurements in beam tests at DESY, probing different scintillator tile sizes. In addition, we introduce measurement methods that allow to observe the time structure of the scintillation process, the time structure of the light collection in the scintillator tile, and the response of the SiPM and measurement electronics separately.

1.1 Experimental Equipment

Modules based on a single SiPM-on-tile element were developed for the CALICE T3B experiment [7]. These modules were further developed and used within the CLAWS project for beam background studies and a beam abort system for the SuperKEKB collider [8–10]. For the measurements discussed in this publication, we used the latest iteration of the CLAWS boards, the phase 3 CLAWS shown in figure 1. Each boards contains a single SiPM under a plastic scintillator tile, as well as the corresponding amplifier electronics allow an analog transmission of the sensor signals over extended distances.

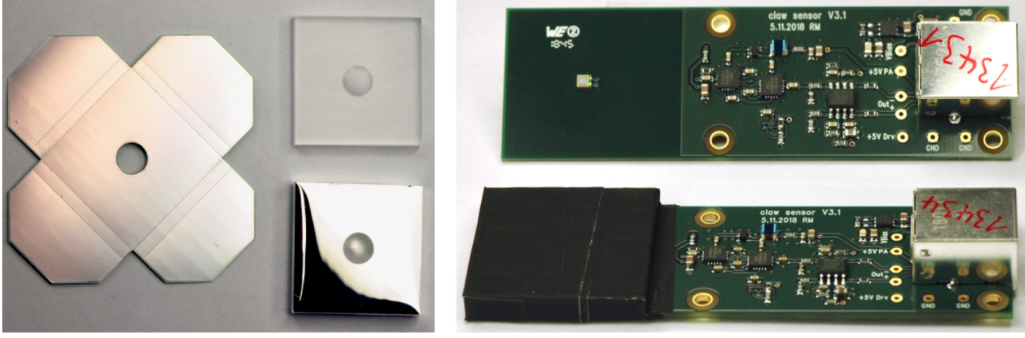


Figure 1: Left: An AHCAL-style scintillator tile of size $30 \times 30 \times 3 \text{ mm}^3$ with a dimple for the SiPM and reflective wrapping foil. Right: Two CLAWS boards, the upper one without scintillator, the lower one with a scintillator. The scintillator tile is fixed with black tape, which also shields from ambient light.

The analog signals are transmitted over CAT6a ethernet cables, which are also used to provide the supply voltage for the amplifier circuit and the bias voltage of the SiPM. The full signal waveforms of each event are recorded with a PicoScope 6804E digital computer-controlled oscilloscope [11].

The SiPMs installed on the CLAWS boards are Hamamatsu S13360-1325PE [12], the same that are used in the AHCAL technological prototype [5].

The plastic scintillator tiles are packed in 3M Vikuiti Enhanced Specular Reflector (ESR) foil to increase the light collection efficiency. Black tape is used to mount the scintillator tile to the claws board and as a stray light protection.

Unlike the scintillators in the AHCAL, which are made of injection-moulded polystyrene, for the present study general-purpose plastic scintillator BC408 [13] is used, because this material is easily available and can be machined into different sizes. We investigated the time resolution of three different scintillator tile sizes $20 \times 20 \times 3 \text{ mm}^3$, $30 \times 30 \times 3 \text{ mm}^3$ and $40 \times 40 \times 3 \text{ mm}^3$. Note

that the dimension of the dimple is the same in all three cases. Drawings of the tile dimensions can be found in [14].

An additional advantage of BC408 is that its properties are well known, which allows us to model the SiPM-on-tile setup in a Geant4 simulation. The results of the simulation will be discussed in an upcoming publication.

1.2 Breaking Down the Signal Creation

In a SiPM-on-tile configuration, detecting a charged particle involves three subsequent steps:

1. The particle deposits energy in the **scintillator** and photons are emitted.
2. The photons propagate through the scintillator tile, and might be reflected at the foil or the tile surface. The term **light collection** summarises all the effects that influence the way of the photons from the scintillation spot to the SiPM.
3. The photons that reach the SiPM can cause an avalanche in one of the pixels. The response of a single pixel is called photoelectron or p.e. The electrical signal is then amplified and measured with the oscilloscope.

Note that all three of these processes potentially have an inherent time structure that influences the time resolution achievable with the SiPM-on-tile configuration.

To understand these processes at a deeper level, multiple different measurement concepts are required. Naturally, the test beam measurements include all three steps of signal creation. Using a small scintillator cube without reflective foil, we can reduce geometric effects and estimate the emission times of the material without light collection. To eliminate the effects from scintillation, we can use pulsed laser light as an alternative light source.

All these measurements are however sensitive to step 3, the light detection and DAQ. Therefore, the impact of the SiPM and measurement electronics is measured separately by shooting short laser pulses directly at the SiPM and measuring the response.

Figure 2 illustrates the three signal creation steps as well as the different measurement methods. The following section 2 shows our test beam measurements. Section 3 discusses the timing properties of BC408 measured with small scintillator cubes, and the laser measurements are presented in section 4.

2 Test Beam Measurements

Measurements with high-energy charged particles involve all three steps of signal creation (scintillation, light collection and light detection at the SiPM). We used electrons with an energy of 3 GeV at DESY's test beam facility [15]. In two test beam weeks of the CALICE AHCAL group, in October 2020 and 2021, we placed our timing setup in front of the AHCAL prototype, such that both experiments used the same electron beam.

The two main observables of these measurements are the **light yield** and the **time resolution** of each SiPM-on-tile configuration. The light yield is defined as the most probable number of photoelectrons (p.e.) measured at the SiPM for a minimum ionising particle in the detector. The time resolution is derived from the hit times reconstructed from individual waveforms recorded in the detectors, as discussed in further detail below.

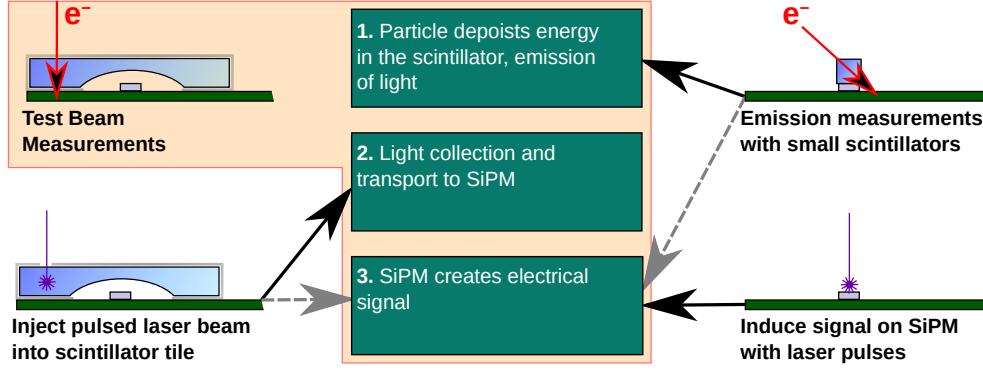


Figure 2: Illustration of the three steps that it takes to generate a signal in a SiPM-on-tile configuration, and the different measurement methods designed to investigate these steps separately.

2.1 Experimental Setup

The timing setup that we used during the test beam measurements is a "beam telescope" made of four scintillator tiles as shown in figure 3. The two outer scintillator tiles (channels A and G) are used for a coincidence trigger, and the two inner scintillator tiles (channels C and E) are used to calculate the time resolution.

In the first test beam campaign in October 2020 all four channels were recorded and the coincidence trigger was generated internally in the oscilloscope. The voltage resolution was 8 bit in a range from -1 V to $+1$ V and the trigger level was set to an equivalent of approximately 2.5 p.e. For each event we recorded 500 pre-trigger and 1000 post-trigger samples, with a sampling time of 0.4 ns. This resulted in an overall time range of 600 ns for each waveform.

In the second test beam campaign in October 2021 we additionally employed a Keysight P9242A oscilloscope to provide an external trigger for the PicoScope. This means that only the data channels C and E were recorded, at the benefit of a higher sampling time of 0.2 ns. In the analysis of this data set, an effective sampling time of 0.4 ns was used. Voltage and trigger settings were left unchanged with respect to the first test beam campaign.

Table 1 summarises the measurement settings of the data used in this publication.

The measurements are controlled by a python script that regularly (approximately every 5 minutes) interrupts for calibration. A calibration run is a separate measurement where each channel is recorded individually, one after another. The trigger level is set to approximately 0.5 p.e which means that it triggers mostly on dark counts where a single pixel of the SiPM fired. Accordingly, the voltage range is set to ± 50 mV. These calibration measurements allow the monitoring of the 1 p.e. signal, and with that the stability of the SiPM gain for each channel. The integral of the calibration waveforms is used to estimate the number of photoelectrons for the recorded signal waveforms.

2.2 Results: Light Yield

The light yield of a detector module is defined as the most probable number of photoelectrons measured at the SiPM for minimum ionization (1 MIP of energy deposition) in the scintillator tile. The light yield is the most probable signal area of a minimum ionizing particle signal divided by

Table 1: Summary of measurement runs used to characterise the SiPM-on-tile with BC408 plastic scintillator tiles. The normal measurement runs, listed in the first three lines, are regularly interrupted for calibration runs where the 1 p.e. peaks of each channel are recorded separately.

Tile Size	Trigger Size	Voltage res.	Trigger	Date
$20 \times 20 \times 3 \text{ mm}^3$	$20 \times 20 \times 3 \text{ mm}^3$	$\pm 1 \text{ V}$, 8 bit	External	October 2021
$30 \times 30 \times 3 \text{ mm}^3$	$30 \times 30 \times 3 \text{ mm}^3$	$\pm 1 \text{ V}$, 8 bit	Internal	October 2020
$40 \times 40 \times 3 \text{ mm}^3$	$30 \times 30 \times 3 \text{ mm}^3$	$\pm 1 \text{ V}$, 8 bit	External	October 2021
Calibration	Trigger on 1 p.e. peak	$\pm 50 \text{ mV}$, 8 bit	Internal	

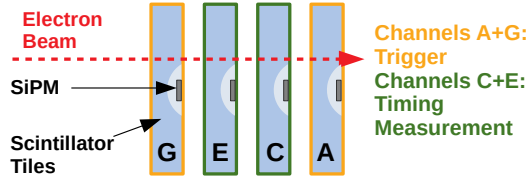


Figure 3: Arrangement of four scintillator tiles during beam test measurements for the SiPM-on-tile timing study

the area of a 1 p.e. signal.

$$LY = \frac{area_{MIP}}{area_{1 \text{ p.e.}}} \quad (2.1)$$

The area of a 1 p.e. signal is extracted from the calibration measurement of each channel using a Gaussian fit as shown in figure 4(d). There are a few counts at the double signal area, which arise from cross-talk or after pulses following a thermally excited 1 p.e. pulse.

Figure 4(a)-4(c) shows the distributions of the signal areas, corresponding to the energy deposition in the scintillator tiles, for charged particles at the test beam. The hit energy distribution is skewed towards higher energies, and is expected to follow the characteristic behaviour of a Landau distribution.

To extract the most probable energy deposition, we performed a fit to a Landau distribution convoluted with a Gaussian distribution, commonly referred to as "Langauss". The Gaussian part accounts for detector noise and measurement uncertainties. The energy deposition in the smallest $20 \times 20 \times 3 \text{ mm}^3$ scintillator tiles (figure 4(a)) agrees very well with the expected Langauss behaviour.

The distributions for the larger scintillator tiles (figures 4(b) and 4(c)) on the other hand show an excess of events at energies above the minimum ionization peak¹. This can be attributed to events where more than one particle deposits energy in the scintillator tiles. To make sure that no double particle events are included in the analysis, an upper limit for the fit range was set manually before the fit, indicated by the black lines in figure 4. Effectively, these limits correspond to an energy of approximately 1.5 MIP.

¹Especially the run with the $40 \times 40 \times 3 \text{ mm}^3$ scintillator tiles (figure 4(c)) has a high number of multi-particle events, for once because larger tiles have a higher geometric cross section, and on the other hand because a beam collimator with a larger aperture was used during this measurement.

The additional particles can be either additional primary electrons from the test beam, or bremsstrahlung photons. A detailed discussion of the double particle events can be found in [16].

Table 2 shows the resulting light yields in units of p.e./MIP. Manufacturing imperfections and individual fluctuations lead to a variation in the light yield for different detector modules. However, the variation between the data channels is consistent with the light yield variation of 12% (standard deviation) observed in more than 20000 channels of the AHCAL technological prototype [5].

Previous experimental studies show that the light yield scales as $1/\sqrt{A}$, where A is the area of the scintillator tile [14, 17]. This is consistent with our measurements.

Table 2: Light yields in photoelectrons per MIP of the BC408 plastic scintillator tiles measured with the CLAWS boards at the test beam.

Tile size	LY Ch. C (p.e./MIP)	LY Ch. E (p.e./MIP)
$20 \times 20 \times 3 \text{ mm}^3$	33.43 ± 0.13	37.67 ± 0.20
$30 \times 30 \times 3 \text{ mm}^3$	23.54 ± 0.17	19.80 ± 0.14
$40 \times 40 \times 3 \text{ mm}^3$	19.30 ± 0.12	19.42 ± 0.14

2.3 Results: Time Resolution

The first step in calculating the time resolution is to assign a particle hit time to each recorded event on each tile. We decided to use the amplitude-dependent constant fraction method: The point in time where a waveform first crosses 25% of its maximum amplitude is used as the hit time.

To eliminate trigger effects, we calculate the hit time difference between the two channels C and E. Figure 5 shows the correlation between the energy deposition in the scintillator tile and the hit time difference. For this analysis we only use events where the energy deposition is in the same bin in both channels. For each energy bin, we extract the width σ of the hit time distribution with a Gaussian fit.

Hit times outside of the interval $\pm 5 \text{ ns}$ are rejected since they tend to be due to early hits caused by baseline noise on one of the two channels.

Assuming that the hit times of channels C and E are uncorrelated, the time resolution of a single channel can be obtained by dividing the width σ by $\sqrt{2}$. The following calculation is performed separately for each energy bin:

$$\sigma_t = \frac{\sigma(t_C - t_E)}{\sqrt{2}} \quad (2.2)$$

In this study, we assume that the "stochastic term" $\propto 1/\sqrt{E}$, resulting from the statistical nature of photon counting, is the only relevant contribution to the energy-dependent time resolution².

$$\sigma_t(E) = \frac{\sigma_{1MIP}}{\sqrt{E}} \quad (2.3)$$

²Uncertainties often have additional terms that are constant or scale with $1/E$, but if we use a fit function that includes these terms, they are very small or even consistent with zero for our measurement results. It is thus sufficient to discuss the time resolution based only on the stochastic term.

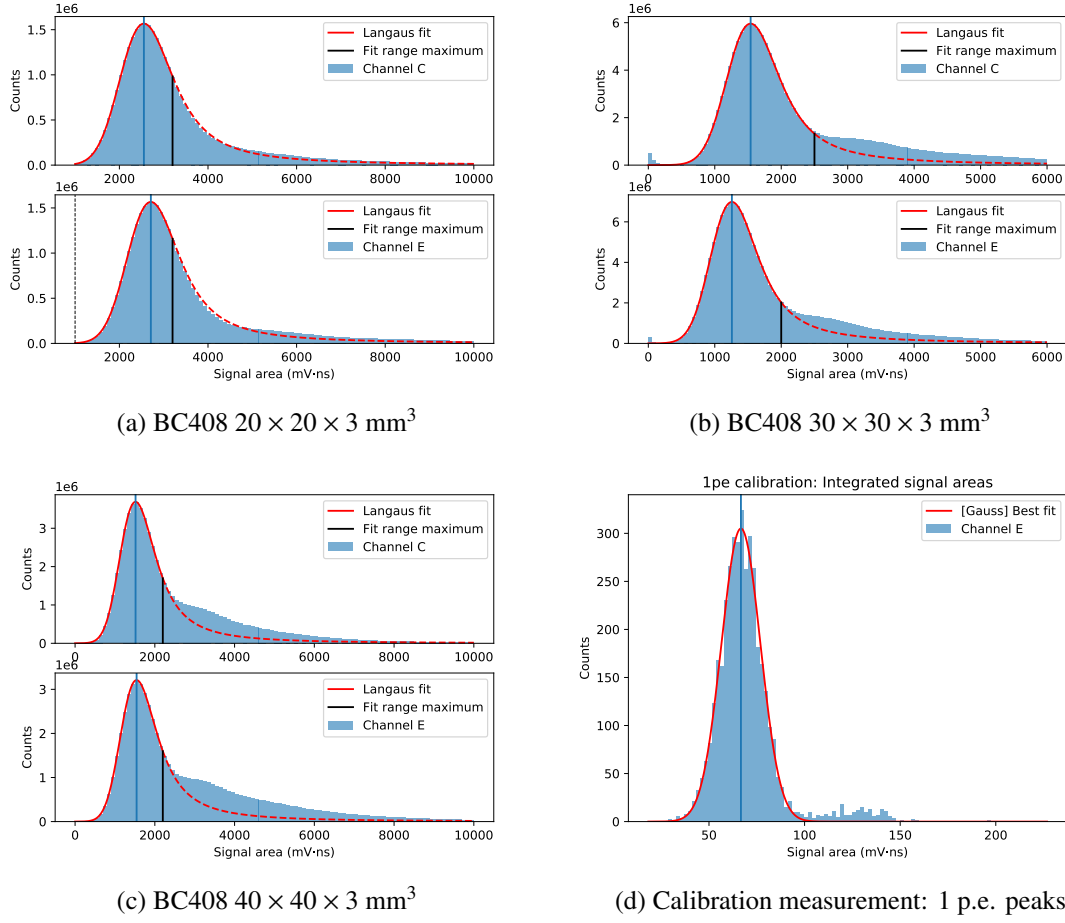


Figure 4: Distributions of the area under the waveform for each channel of the test beam measurements and for a 1 p.e. calibration measurement. A numerical fit with a Landau/Gauss convolution (subfigures a-c), and a Gaussian in (subfigure d) is performed for each distribution. The black vertical lines indicate the maximum of the fit range. The best fit functions is plotted in red.

Figure 6 shows the measured time resolutions for all three scintillator tile sizes as a function of the energy deposition. The solid lines are fits to functions following equation 2.3. The only fit parameter, σ_{1MIP} , is the time resolution for a signal amplitude of 1 MIP. Energy depositions below 1 MIP are excluded from the fit due to the larger uncertainties of those measurement points. Table 3 shows the fit results for σ_{1MIP} .

Both the time resolution and the light yield clearly depend on the scintillator tile size. Since a higher number of photons arriving at the SiPM leads to a better time resolution (as seen in equation 2.3), the time resolution also improves with a higher light yield. This can be part of an explanation why the smaller scintillator tiles have a better time resolution.

The fit results are only valid for one individual pair of scintillator tiles. The expected tile-to-tile variation of 12 % of the light yield results in tile-to-tile fluctuation in time resolution of 6%, if we consider the observed scaling of the time resolution with the square root of the light yield. The right column of table 3 shows the total uncertainty of the time resolution, including tile-to-tile

fluctuations.

Table 3: Single channel time resolution at minimum ionization σ_{1MIP} for different BC408 scintillator tiles measured at the test beam. The total uncertainty includes the uncertainty from the fit as well as expected fluctuations in the time resolution that arise from tile-to-tile differences.

Tile size	σ_{1MIP} (ns)	Fit reduced χ^2	Fit uncertainty (ns)	Total uncertainty (ns)
$20 \times 20 \times 3 \text{ mm}^3$	0.3847	3.10	0.0004	0.023
$30 \times 30 \times 3 \text{ mm}^3$	0.5785	1.54	0.0006	0.035
$40 \times 40 \times 3 \text{ mm}^3$	0.7027	1.76	0.0008	0.042

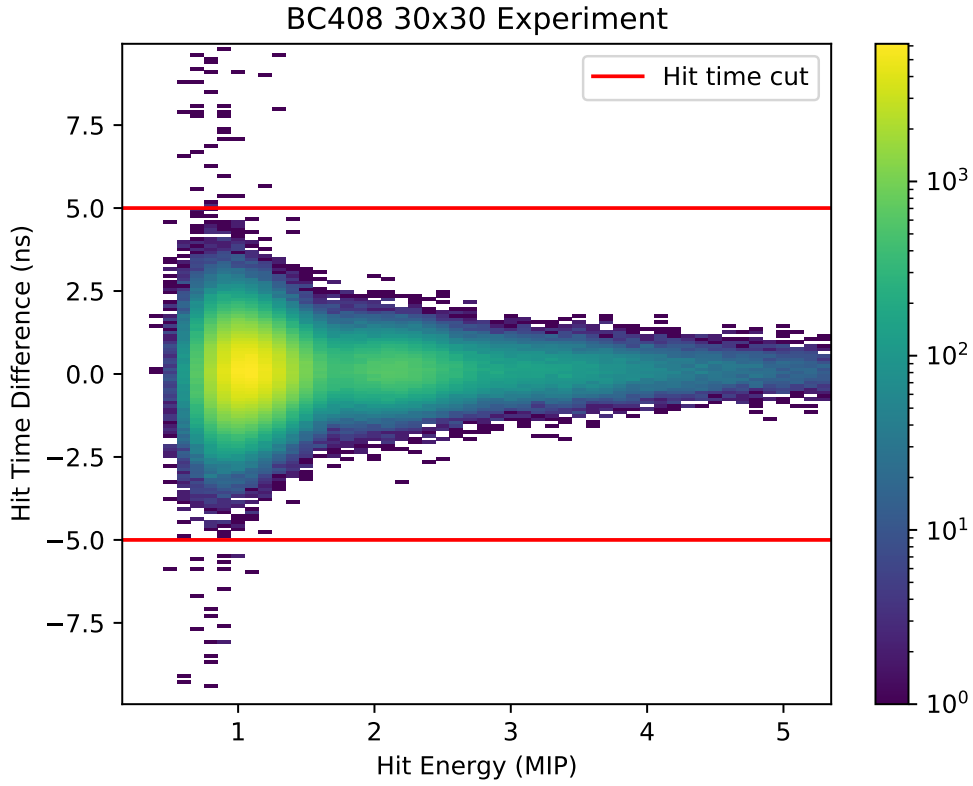


Figure 5: Histogram of hit time difference between the measurement channels and energy deposition in the scintillator for two BC408 $30 \times 30 \times 3 \text{ mm}^3$ scintillator tiles. Hits outside of the red lines are early hits that arise from noise and are rejected in the analysis. Only events with a similar energy deposition in both scintillator tiles are used in this plot.

3 Timing Properties of BC408

The timing properties of the scintillation light emission of the BC408 plastic scintillator are expected to have an important impact on the time resolution of the SiPM-on-tile module. The influence of

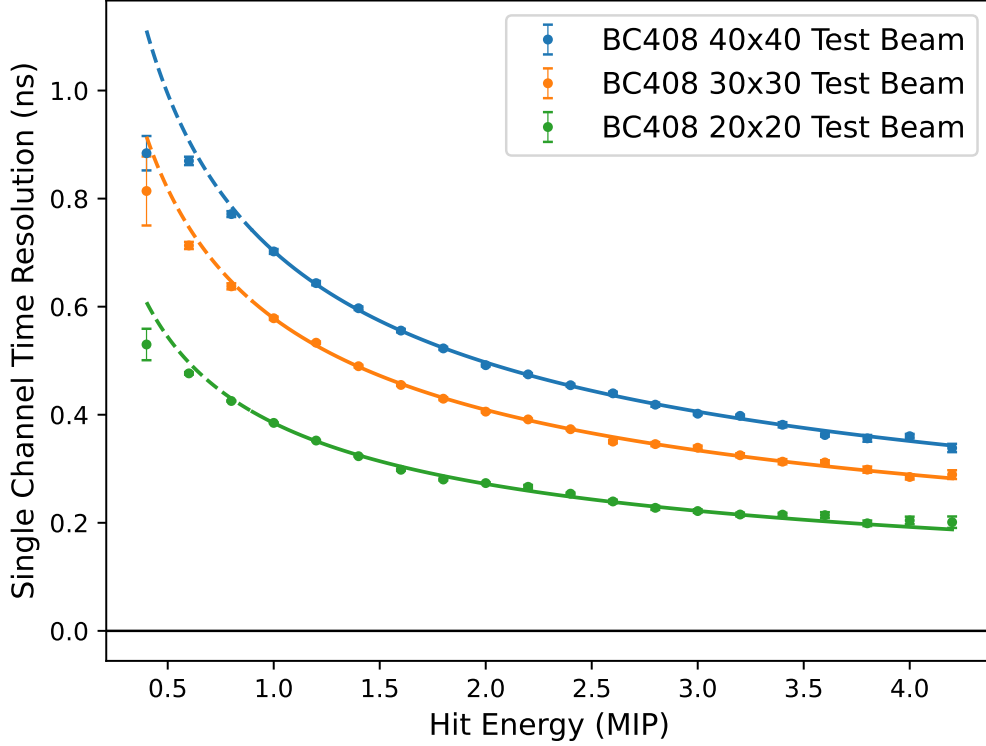


Figure 6: Time resolution of BC408 plastic scintillator tiles as a function of deposited energy in the scintillator. The data points are results of the test beam measurements, the lines are fits to a function following equation 2.3. Only data points at 1 MIP and above are included in the fit. The dashed lines show an extrapolation of the fit function to lower energies.

the scintillator properties can be accessed experimentally by reducing geometric effects in the scintillator as far as possible.

3.1 Experimental Setup

For measuring the timing properties of BC408, we use a setup that is designed to avoid geometric effects as far as possible and only detects light directly emitted from the scintillator. Scintillator cubes measuring $5 \times 5 \times 5 \text{ mm}^3$ are used instead of larger tiles to minimize the path that photons travel. Instead of ESR foil, the cubes are wrapped in black foil to suppress multiple reflections. The scintillator cubes are excited using electrons from a ^{90}Sr source. The signal of one cube is used for the timing analysis, and the second cube is used to provide a coincidence of two cubes as a trigger signal. This ensures full penetration of the first cube, and thus scintillation light emission over the full depth of the scintillator element. The measurement setup is illustrated in figure 7, and the measurement settings are summarised in table 4.

Since there is only one measurement channel, it is not possible to calculate the time resolution from a hit time difference. Instead we analyze the time structure of each waveform.

Since each photon triggers the same pixel response in the SiPM and the shape of this 1 p.e. signal is known from calibration measurements, the arrival times of single photons at the SiPM can be estimated from the analog waveform measured with the oscilloscope. To this end we have developed a waveform decomposition algorithm, inspired by the signal reconstruction in the T3B experiment [7]. Starting from the measured waveform, the algorithm iteratively subtracts 1 p.e. signals until only the baseline noise remains. The points in time where the 1 p.e. responses were subtracted are used as photon hit times. A detailed description of the waveform decomposition algorithm, as well as a discussion of its performance, can be found in [16].

Table 4: Measurement settings used for determining the timing properties of BC408, and for the laser measurements.

Measurement	Voltage res.	Sampling	Trigger
BC408 $5 \times 5 \times 5 \text{ mm}^3$ cubes	$\pm 500 \text{ mV}$, 8 bit	0.4 ns	Light from first BC408 cube
Laser measurements	$\pm 1 \text{ V}$, 8 bit	0.4 ns	Laser driver

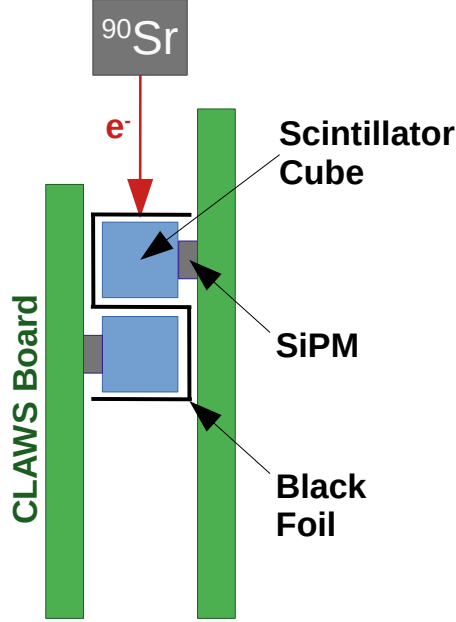


Figure 7: Setup with small scintillator cubes used to mitigate geometric effects when measuring the photon emission time spectrum. The scintillator cubes are made of BC408 and have a dimension of $5 \times 5 \times 5 \text{ mm}^3$. A black foil shields the cubes from ambient stray light and crosstalk. The oscilloscope is configured as a coincidence trigger on both channels.

3.2 Results

The photon emission time distribution of BC408, measured with small scintillator cubes, is shown in figure 8. The red line is a fit to a bi-exponential function as in equation 3.1, convoluted with a Gaussian to account for detector and electronic noise.

$$p(t|\tau_{rise}, \tau_{fall}) = \begin{cases} \exp\left(-\frac{t}{\tau_{fall}}\right) \cdot \left[1 - \exp\left(-\frac{t}{\tau_{rise}}\right)\right] \cdot \frac{\tau_{rise} + \tau_{fall}}{\tau_{fall}^2} & t > 0 \\ 0 & \text{else} \end{cases} \quad (3.1)$$

Table 5 compares the rise and fall times of the BC408 photon emission spectrum, obtained with the fit in figure 8, to the rise and fall times from the BC408 datasheet [13]. Since the manufacturer does not state how their time constants are defined, these values are however not directly comparable.

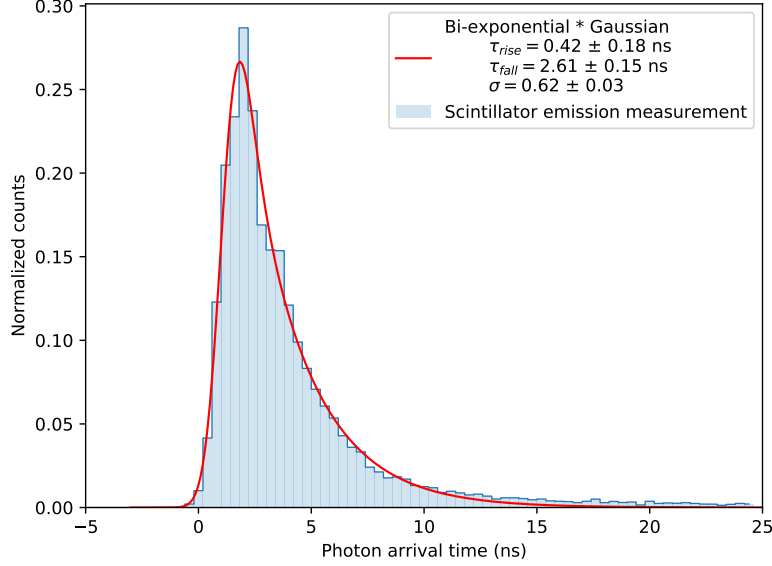


Figure 8: Emission time spectrum of BC408 measured with small scintillator cubes. The photon hit times were extracted by decomposition of the waveform into 1 p.e. peaks (see section 3.1). The solid line is a fit to the bi-exponential function in equation 3.1 convoluted with a Gaussian.

Table 5: Timing properties of the plastic scintillator BC408 as measured in our setup, compared to the manufacturer information from the BC408 datasheet. Note that the numbers are not directly comparable.

	Rise time (ns)	Fall time (ns)
Measured	0.42 ± 0.18	2.61 ± 0.15
Manufacturer information	0.9	2.1

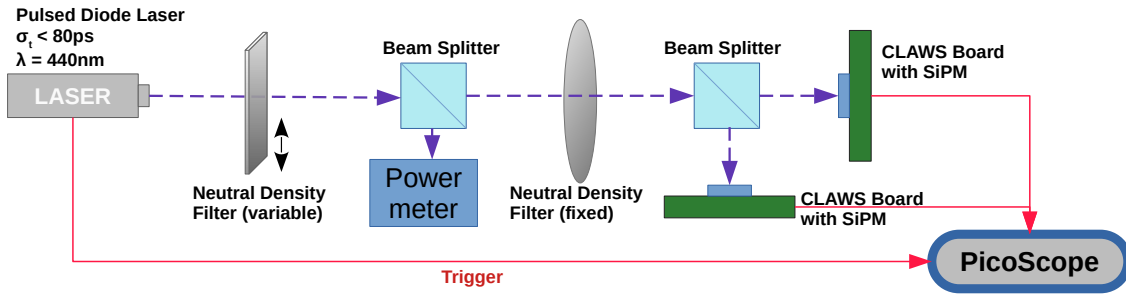
4 Laser Measurements

In addition to scintillation, there are two more processes involved in the signal creation within a SiPM-on-tile setup: light collection and light detection. Light collection means the propagation of scintillation photons through the tile until their absorption by the SiPM. Light detection includes the avalanches in the SiPM and the amplification and measurement of the resulting electrical signal. These two processes can be probed individually by using a pulsed laser as an alternative light source.

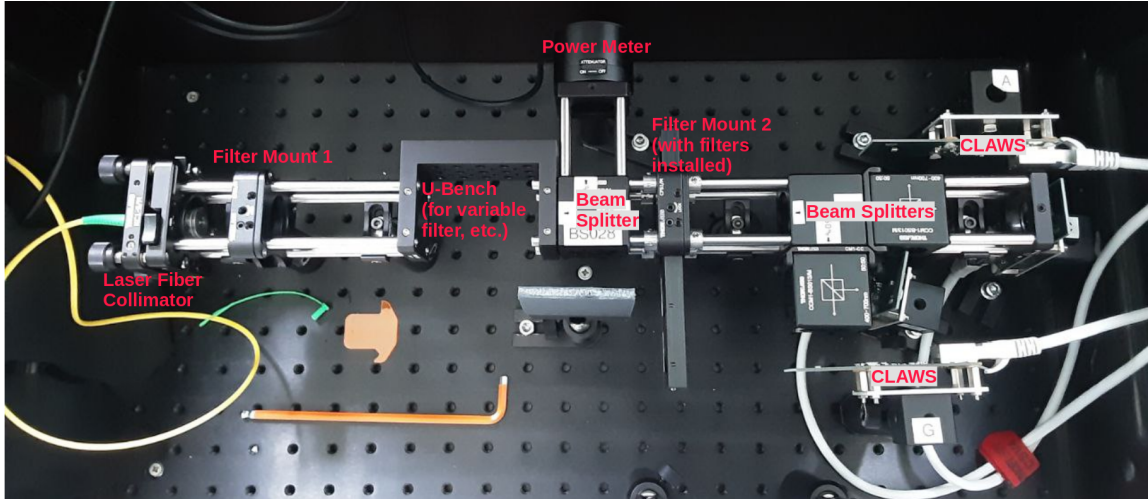
4.1 Experimental Setup

For the laser measurements we used a PicoQuant LDH-P-C-440B pulsed diode laser. Detailed information on the setup can be found in [16]. The wavelength of 440 nm is close to the SiPM's peak sensitivity and similar to the peak emission wavelength of the used scintillator BC408. The pulses are shorter than 80 ps, which is significantly faster than the typical signals that we measure for example at the test beam. The measurement settings are summarised in table 4.

Figure 9 shows an illustration and a photograph of the laser setup. The light intensity that reaches the SiPMs is controlled using a set of neutral density optical filters and is monitored with a power meter. The beam is split and directed to two different SiPMs, which allows to calculate the time resolution from the hit time difference, as described in section 2.3. The trigger signal is directly provided from the laser driver.



(a) Sketch of the setup



(b) Picture of the setup.

Figure 9: Laser setup used to study light collection and light detection in the SiPM-on-tile setup without the impact of scintillation light. Short laser pulses of variable intensity are directed to multiple SiPMs on CLAWS modules simultaneously.

To probe the response of the SiPM and electronics to very short light pulses, the laser beam is aimed directly onto the SiPM. This allows to estimate the timing uncertainty that arises from

the light sensor, the electronics and the data acquisition, i.e. the timing uncertainty of the light detection.

The light collection is probed by injecting short light pulses into the scintillator tile. Since the laser wavelength is close to the emission wavelength of the scintillator, there should be no more fluorescence such that this measurement is only sensitive to the geometric effects of light collection.

4.2 Results: Light Detection and Hardware Response

Figure 10 shows the time resolution of the light detection which was obtained from laser measurements, compared to the time resolution of a $30 \times 30 \times 3 \text{ mm}^3$ scintillator tile at the test beam. If we assume that the timing uncertainty from the electronics and SiPM is uncorrelated to the effects of the scintillator tile (scintillation and light collection), we can write the overall time resolution of the SiPM-on-tile system as

$$\sigma_t = \sigma_{Tile} \oplus \sigma_{SiPM} = \sqrt{\sigma_{Tile}^2 + \sigma_{SiPM}^2} \quad (4.1)$$

The green data points in figure 10 are the time resolution of the test beam measurement *without* the uncertainties induced by the time resolution of the SiPM:

$$\sigma_{Tile} = \sigma_t \ominus \sigma_{SiPM} = \sqrt{\sigma_t^2 - \sigma_{SiPM}^2} \quad (4.2)$$

Since the timing uncertainty of electronics and SiPM is almost an order of magnitude lower than the overall time resolution, and since uncertainties are added in quadrature, this impact is negligible in our measurements.

This can also be seen the time distribution of photons arriving at the SiPM, shown in figure 11. Compared to the time distribution of scintillation photons, the laser measurement yields a very short time distribution. Further discussion on this plot can be found in [16].

All in all, the laser measurements show that the SiPM, CLAWS, amplifier electronics and oscilloscope together are still significantly faster than other signal parts. Therefore, the contribution of the hardware to the time structure of the measured signals can be neglected.

4.3 Results: Light Collection

Since the electronics and light detection do not contribute significantly to the overall timing properties of the signals that we observe at the test beam, the two remaining processes are light collection and scintillation. The upper panel of figure 12 shows the photon time distributions of these two processes for a BC408 $30 \times 30 \times 3 \text{ mm}^3$ scintillator tile: The light collection was measured with the laser setup and the scintillation histogram is the same as in figure 8.

The lower panel of figure 12 shows the photon time distribution for a BC408 $30 \times 30 \times 3 \text{ mm}^3$ tile measured at the test beam. The time structure of the test beam signals agrees very well with the red line, which is a convolution of the scintillation and light collection distributions from the upper plot.

This demonstrates that the signals that we observe at the test beam are indeed determined by scintillation and light collection together. The comparison shown in figure 12 works equally well for the scintillator sizes $20 \times 20 \times 3 \text{ mm}^3$ and $40 \times 40 \times 3 \text{ mm}^3$, and can be found in [16].

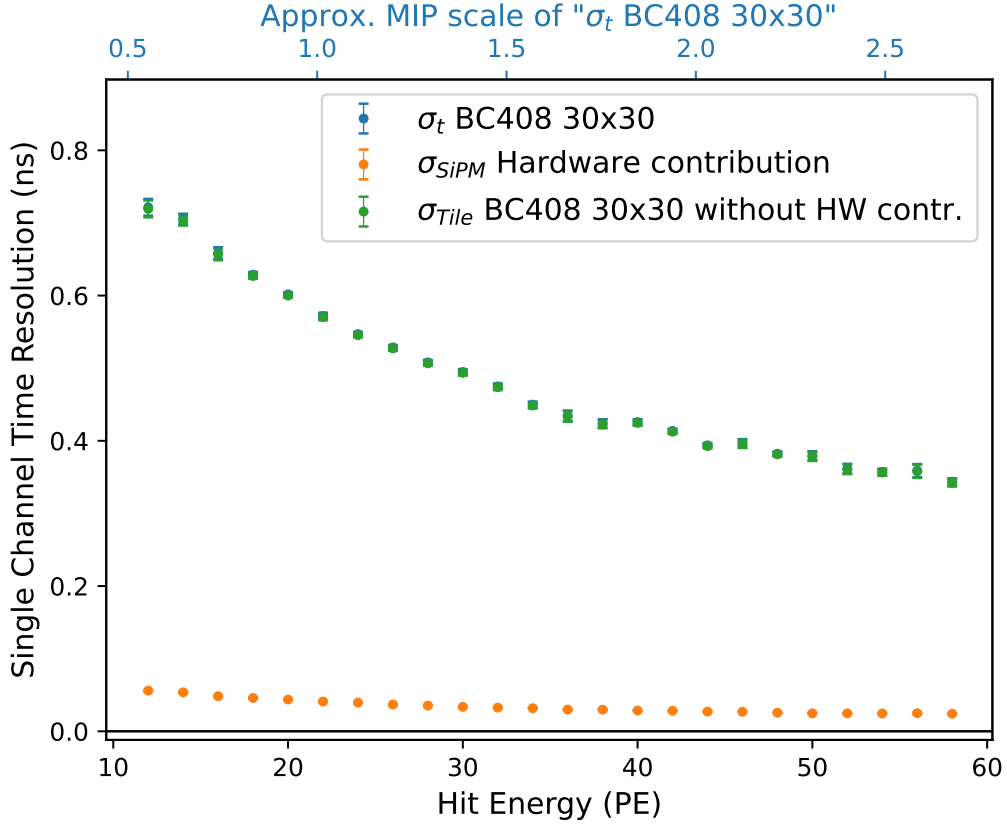


Figure 10: The energy dependent time resolution of a test beam measurement with BC408 $30 \times 30 \times 3 \text{ mm}^3$ scintillator tiles is compared to the time resolution obtained from short laser pulses aimed directly at the SiPM, which is essentially the time resolution of the SiPM and electronics. The green curve is the computed time resolution of the test beam measurement without the timing uncertainties of the SiPM. The common energy scale is photoelectrons, and for reference the MIP scale of the test beam measurement is shown at the top axis.

The light collection is a geometric effect that arises from the different paths that photons travel in the scintillator tile. Figure 13 compares the photon time distribution for the light collection measurements with a laser on three different scintillator tile sizes. There is clearly a different time structure for these three geometries, with smaller tiles responding faster. This suggests that the reason why the time resolution of the SiPM-on-tile setup depends on the geometry of the scintillator tile is not only the light yield, but also the time response arising from different light paths in the scintillator.

5 Conclusions

Using DESY's test beam facility, we have measured the light yields and time resolutions of SiPM-on-tile configurations with three different scintillator tile sizes, all made of the plastic scintillator BC408 with a thickness of 3 mm. The time resolution for an energy deposition corresponding to

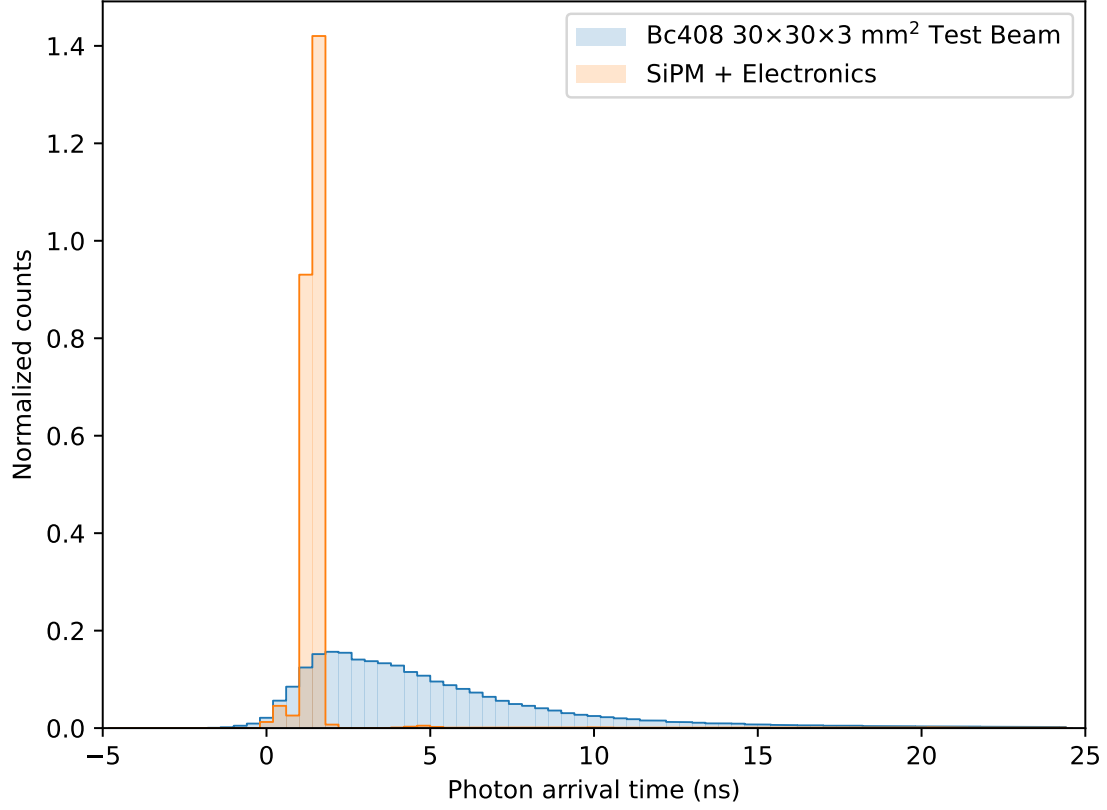


Figure 11: Time distribution of photoelectrons measured at the SiPM. The orange histogram is the time distribution of the SiPM and electronics, triggered by short laser pulses. The time distribution of scintillation photons from a test beam measurement is shown in blue. The photon hit times were extracted by decomposition of the waveform into 1 p.e. peaks (see section 3.1).

minimum ionization is determined with a numerical fit to the energy-dependent time resolution. In addition to the fit uncertainty we include a 6% fluctuation for the final value of the time resolution that we expect to arise from individual tile-to-tile fluctuations. The measured time resolutions are

- $\sigma_t = 0.38 \pm 0.02$ for $20 \times 20 \times 3 \text{ mm}^3$ scintillator tiles,
- $\sigma_t = 0.58 \pm 0.04$ for $30 \times 30 \times 3 \text{ mm}^3$, and
- $\sigma_t = 0.70 \pm 0.04$ for $40 \times 40 \times 3 \text{ mm}^3$.

for an energy deposition corresponding to the most probable value of a minimum-ionizing particle. The time resolution scales with the inverse of the square root of the signal amplitude.

In order to disentangle the contributions of scintillation, light collection and light detection to the timing properties, we have developed different measurement methods where the signals are created using electrons from a radioactive ^{90}Sr source or pulsed laser light.

These complementary measurements show that our SiPM, electronics and digitisation are fast enough to have no impact on our measurement results. Instead, the time structure observed

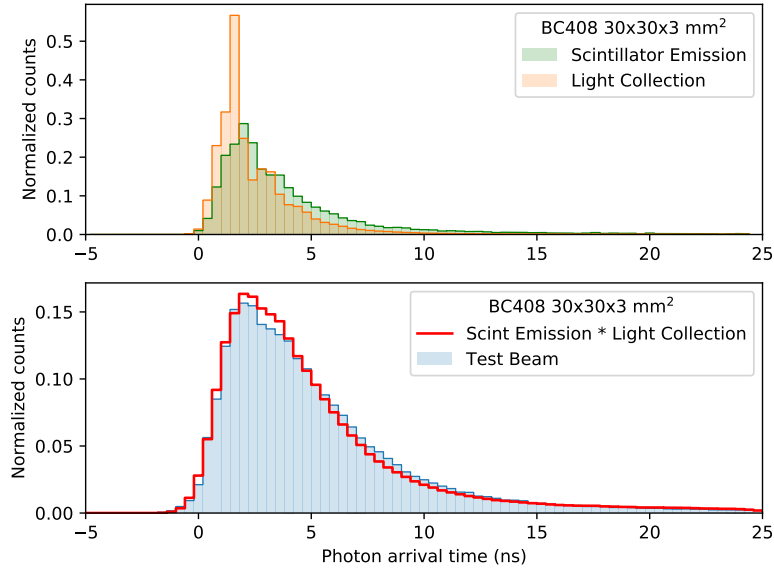


Figure 12: Top: Photoelectron time distribution of scintillation and light collection for BC408 $30 \times 30 \times 3 \text{ mm}^3$ scintillator tiles. Bottom: Photoelectron time spectrum observed at the test beam with the same tile geometry, and a convolution of scintillation and light collection. The photon hit times were extracted by decomposition of the waveform into 1 p.e. peaks (see section 3.1).

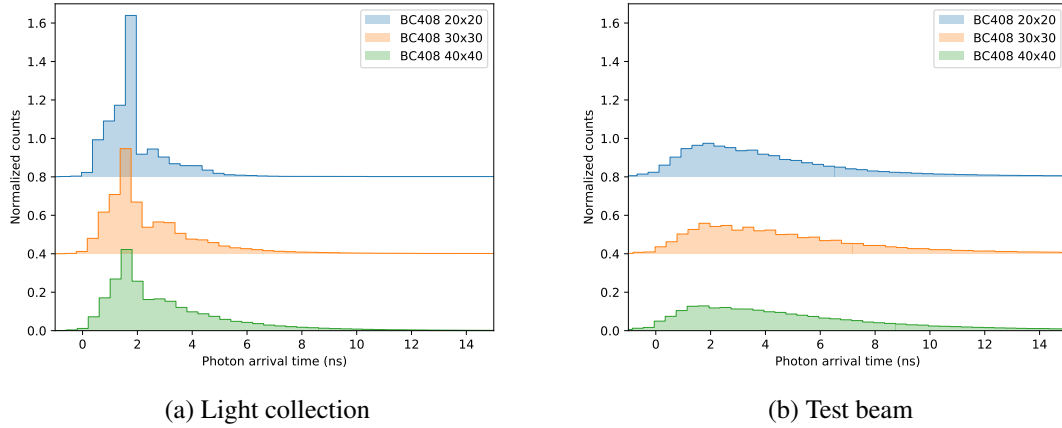


Figure 13: Photoelectron time distribution obtained at test beam measurements (right) and from light collection only (left) for different scintillator tile sizes. The photon hit times were extracted by decomposition of the waveform into 1 p.e. peaks (see section 3.1).

in a SiPM-on-tile configuration can be fully described in terms of the scintillation and the light propagation in the scintillator tile.

The analysis of test beam data shows that the time resolution strongly depends on the energy deposition in the scintillator tile, and thus also on the light yield. The light yield in turn depends on the scintillator tile size. Moreover, the laser measurements suggest that the light collection in the

scintillator tile also has a time structure that depends on the scintillator tile size.

This motivates to further study the timing properties of the SiPM-on-tile technology, and specifically how the scintillator tile size, the light yield, and the time resolution are correlated. In an upcoming publication these open questions will be addressed with a Geant4-based simulation of the SiPM-on-tile setup.

Acknowledgements

We thank our colleagues in the CALICE Collaboration for helpful discussions.

This project has received funding from the European Union’s Horizon 2020 Research and Innovation programme under Grant Agreements no. 654168 and no. 101004761.

The measurements leading to these results have been performed at the Test Beam Facility at DESY Hamburg (Germany), a member of the Helmholtz Association (HGF).

References

- [1] N. Akchurin, C. Cowden, J. Damgov, A. Hussain and S. Kunori, *On the use of neural networks for energy reconstruction in high-granularity calorimeters*, *JINST* **16** (2021) P12036, [[arXiv:2107.10207](#)].
- [2] C. Graf and F. Simon, *Time-assisted energy reconstruction in a highly-granular hadronic calorimeter*, *JINST* **17** (2022) P08027, [[arXiv:2203.01317](#)].
- [3] S. V. Chekanov et al., *Precision timing for collider-experiment-based calorimetry*, [arXiv:2203.07286](#).
- [4] F. Simon, *Silicon Photomultipliers in Particle and Nuclear Physics*, *Nucl.Instrum.Meth. A* **926** (May, 2019) 85–100, [[arXiv:1811.03877v2](#)].
- [5] CALICE collaboration, A. White et al., *Design, construction and commissioning of a technological prototype of a highly granular SiPM-on-tile scintillator-steel hadronic calorimeter*, *JINST* **18** (2023) P11018, [[arXiv:2209.15327](#)].
- [6] CMS collaboration, *The Phase-2 Upgrade of the CMS Endcap Calorimeter*, tech. rep., CERN, Geneva, Nov, 2017.
- [7] F. Simon, C. Soldner and L. Weuste, *T3B — an experiment to measure the time structure of hadronic showers*, *JINST* **8** (Sep, 2013) P12001. 18 p, [[arXiv:1309.6143](#)].
- [8] M. Gabriel et al., *A time resolved study of injection backgrounds during the first commissioning phase of SuperKEKB*, *Eur. Phys. J. C* **81** (2021) 972, [[arXiv:2012.10948](#)].
- [9] M. Gabriel, *CLAWS - a novel time resolved study of backgrounds during the first commissioning phase of SuperKEKB*. PhD thesis, TU Munich, November, 2019.
- [10] H. U. Windel, *CLAWS – An Injection Background Monitoring System for the Second and Third Phase of the SuperKEKB Commissioning*. PhD thesis, TU Munich, September, 2021.
- [11] Pico Technology, *PicoScope 6000E Series Datasheet*, <https://www.picotech.com/download/datasheets/picoscope-6000e-series-data-sheet.pdf>.
- [12] Hamamatsu Photonics, *SiPM S13360-1325PE Datasheet*, <https://www.hamamatsu.com/eu/en/product/type/S13360-1325PE/index.html>.

- [13] Luxium Solutions, *BC-400, BC-404, BC-408, BC-412, BC-416 Datasheet*,
https://www.luxiumsolutions.com/sites/default/files/2023-08/146337_Luxium_SGC%20BC400%20404%20408%20412%20416_FIN.pdf .
- [14] L. de Silva and F. Simon, *Effects of misalignment on response uniformity of sipm-on-tile technology for highly granular calorimeters*, *Journal of Instrumentation* **15** (Jun, 2020) P06030–P06030.
- [15] R. Diener, J. Dreyling-Eschweiler, H. Ehrlichmann, I.-M. Gregor, U. Kötz, U. Krämer et al., *The DESY II Test Beam Facility*, Oct., 2018. 10.1016/j.nima.2018.11.133.
- [16] F. Hummer, *Intrinsic time resolution of plastic scintillator tiles with sipm readout for highly granular calorimeters*, Master’s thesis, TU Munich, March, 2022.
- [17] A. Belloni, Y. Chen, A. Dyshkant, T. Edberg, S. Eno, J. Freeman et al., *Test beam study of sipm-on-tile configurations*, *Journal of Instrumentation* **16** (Jul, 2021) P07022.